THE ASTROPHYSICAL JOURNAL, 319:730–741, 1987 August 15

MASS, LUMINOSITY, AND LINE WIDTH RELATIONS OF GALACTIC MOLECULAR CLOUDS

P. M. SOLOMON, A. R. RIVOLO, J. BARRETT, AND A. YAHIL
Astronomy Program, State University of New York–Stony Brook
Received 1986 October 2; accepted 1987 February 2

ABSTRACT

We present measurements of the velocity line width, size, virial mass, and CO luminosity for 273 molecular clouds in the Galactic disk between longitudes of 8° and 90°. These are obtained from three-dimensional data in the Massachusetts–Stony Brook CO Galactic Plane Survey. From an analysis of these measurements we show that the molecular clouds are in or near virial equilibrium and are not confined by pressure equilibrium with a warm or hot phase of interstellar matter. The velocity line width is shown to be proportional to the 0.5 power of the size, $\sigma_v \propto S^{0.5}$. Combined with virial equilibrium, this shows that the clouds are characterized by a constant mean surface density of 170 $M_\odot$ pc^{-2} and have a mass $M \propto \sigma_v^4$. A tight relationship, over four orders of magnitude, is found between the cloud dynamical mass, as measured by the virial theorem, and the CO luminosity $M \propto (L_{CO})^{0.81}$. This relationship establishes a calibration for measuring the total molecular cloud mass from CO luminosity for individual clouds and for the Galactic disk. The cloud CO luminosity is $L_{CO} \propto \sigma_v^5$, which is the molecular cloud analog of the Tully-Fisher or Faber-Jackson law for galaxies.

The mass-luminosity law is accounted for by a cloud model consisting of a large number of optically thick clumps in virial equilibrium, each with a thermal internal velocity dispersion, but with the clouds effectively optically thin at a fixed velocity along the line of sight. The typical clump mass is of order a stellar mass and approximately equal to the Jeans mass at the clump density and thermal velocity dispersion.

Subject headings: interstellar: molecules — galaxies: Milky Way

I. INTRODUCTION

The identification of molecular clouds in the inner Galaxy, from CO emission contours, has led to the conclusion (Solomon, Sanders, and Scoville 1979; Solomon and Sanders 1980) that most of the mass in the molecular interstellar medium is in the form of clouds with diameters greater than 20 pc and masses greater than 10^5 $M_\odot$ which were named *giant molecular clouds* (GMCs). The high abundance and weak dipole moment of CO make the millimeter rotational lines by far the best available tracers of molecular hydrogen. The minimum local density of $n(H_2) \approx 100$ cm^{-3} required to excite the $J = 1 \rightarrow 0$ line appears to be well matched to the densities of giant molecular clouds.

From a sample of 38 clouds, defined as closed contours at a radiation temperature $T_R^* = 3$ K in longitude-velocity space at a fixed latitude ($23° < l < 30°$, $b = 0°$), Solomon, Sanders, and Scoville (1979) and Solomon and Sanders (1980) obtained a spectrum of cloud sizes ranging from 15 to 90 pc. The mass-fraction distribution was shown to have a positive index with half of the total mass contained in clouds with diameters larger than $\sim$60 pc and mass greater than or equal to 10^6 $M_\odot$. A similar analysis of longitude-velocity contours, using ^{13}CO emission (Liszt, Xiang, and Burton 1981), also showed that the mass-fraction spectrum has a positive idex but with the largest clouds being of order 50 pc in size. From ^{13}CO two-dimensional maps of three fields, each 1° square, Stark (1979) found the emission dominated by large clouds in two of three fields. More recently, 80 clouds were identified from latitude-velocity contours (Sanders, Scoville, and Solomon 1985) yielding a size and mass spectrum having half the total mass in clouds larger than 48 pc and masses greater than $5(10)^5$ $M_\odot$. Dame (1984), Dame *et al.* (1986), Myers *et al.* (1986), and Cohen *et al.* (1985) have analyzed the two-dimensional, low-resolution Goddard Institute for Space Studies (GISS) CO survey and found, after subtracting a "background," about 30 giant cloud complexes in the northern inner Galaxy and 37 in the southern Carina arm with typical masses of 10^6 $M_\odot$.

While there is general agreement among these recent surveys as to the gross properties of giant molecular clouds, these previous studies have all been unable adequately to define and measure the physical properties and the distribution of most of the molecular clouds in the inner Galaxy. The reason for this shortcoming has been that the data were taken either with high spatial resolution, but very wide (12′) sampling (Sanders, Scoville, and Solomon 1985), or with complete sampling, but with resolution too low (8′) to resolve typical inner Galaxy clouds (Dame *et al.* 1986; Meyers *et al.* 1986; Cohen *et al.* 1985).

In this paper we present an analysis of cloud sizes, velocity line widths, viral masses, and CO luminosities which utilizes the higher resolution Massachusetts–Stony Brook Galactic plane CO survey. This survey has approximately 20 times the area sampling of Sanders, Scoville, and Solomon (1985) and to 10 times that of the Dame *et al.* (1986) survey.

II. OBSERVATIONS AND CLOUD DEFINITION

The survey observations were carried out during 1981 and 1982 on the FCRAO 14 m antenna operating at a frequency of 115.271 GHz (HPFW = 47″). Approximately 40,000 CO spectra were obtained between the limits of 8° to 90° in longitude, $-1°$ to $+1°$ in latitude, and -100 to $+200$ km s^{-1} in velocity, with a typical rms noise level of 0.35 K. The survey spacing of 3′ (over the range $l = 18°$–$54°$) was chosen to enable measurement of essentially all molecular clouds inside the solar circle with size greater than 20 pc. For example, on the far side of the Galaxy (with respect to the tangent point) at distances of 14 kpc the spacing is 13 pc; on the near side, in the molecular ring at a distance of 4 kpc, the spacing is 3.5 pc. A more complete discussion of the observations and calibration

procedures, along with maps of the complete data in latitude-velocity space, is in Sanders *et al.* (1986). Longitude-velocity maps and spatial (longitude-latitude) maps at fixed velocities are given in Clemens *et al.* (1986) and Solomon *et al.* (1987). Inspection of the actual survey contours in the above references shows that many clouds easily stand out from the background and can be defined with little difficulty. However, there are also regions of strong emission where blending of features in the three-dimensional l, b, v space complicates the definition of clouds, and results are subject to different interpretations by different observers. In order to obtain a cloud data set in an objective manner we have adopted a procedure which unambiguously defines cloud boundaries in three dimensions.

Clouds are defined as topologically closed surfaces of antenna temperature, T_R^*, in the three-dimensional space l, b, v. Clouds can be defined at any intensity level. Typical values for boundary intensities are $T_{\rm min} = 3, 4, 5, 6, 7$ K. Thus each spatial point within the boundary has a peak intensity greater than $T_{\rm min}$. The Galactic plane emission is thus broken up into a set of discrete clouds for each minimum intensity. For the purpose of this analysis a cloud was required to have a minimum total integrated intensity summed over all locations inside the surface of 40 K km s^{-1} for $T_{\rm min} = 6$ and 7 K and 60 K km s^{-1} for $T_{\rm min} = 4$ and 5 K. For each value of $T_{\rm min}$ chosen there is a corresponding population containing about 400 clouds. Typically there are about 1000 clouds smaller than the minimum integrated intensity. Large sections of the galactic plane are blended at the 3 K level with features extending over as much as 5° and 60 km s^{-1}. By contrast there is very little blending of the surfaces at the 6 K level. The 4 K list was adopted except for the confused regions between longitudes of 8° and 32° and velocities $v > 60$ km s^{-1}. Here a selection was made of the lowest intensity surface which was not severely blended. The area quadrupole moment (in l, b) of each cloud was used as a quantitative measure of the cloud asymmetry to eliminate spatially blended clouds. The final catalog presented in this paper thus consists of a mixture of clouds defined at the $T_{\rm min} = 4$, 5, 6, or (in a few cases) 7 K level. A complete list of all clouds at $T_{\rm min} = 3, 4, 5, 6, 7$ K will be published separately. Above longitudes of 54°, where the emission is weaker, the 3 K cloud boundaries were substituted for the 4 K clouds, but only if the cloud met the size criteria at 4 K.

The catalog is tabulated in Table 1. Each cloud in the catalog is described by a set of parameters including: the cloud boundary intensity $T_{\rm min}$ and an index "I" referring to its number on the appropriate list, location of the emission peak in l, b, v space, peak line intensity T_p, Galactocentric radius R, (determined from circular rotation), distance from the Sun D, height from Galactic plane z, the rms dispersions from the means in all three coordinates σ_l, σ_b, σ_v, the CO luminosity $L_{\rm CO}$, and the virial theorem mass $M_{\rm VT}$. The location of the peak line intensity is not necessarily the location of peak integrated intensity. The dispersions were computed from the intensity-weighted variances over all elements $T(l, b, v)$ within the clouds. Explicitly $\sigma_x = (\langle x^2\rangle - \langle x\rangle^2)^{1/2}$, $\langle x\rangle = \sum_i T_i x / \sum_i T_i$, $x = l, b, v$. Since a meaningful measure of dispersion requires a minimum cloud size, we accepted for the catalog only those clouds with a total number of l, b, v elements greater than 25 above the boundary intensity. The last column in Table 1 contains flags describing distance assignment (N = near, F = far) and method used. Clouds flagged with an "X" fit the kinematics of the 3 kpc expanding arm (see, e.g., Cohen and Davis 1976). In addition to the parameters in Table 1 each cloud has maximum extents in l, b, v which define a "box" circumscribing the true cloud boundaries. In computing the dispersions, σ_l, σ_b, σ_v, and the total cloud luminosities we have included all emission down to the 1 K level within the cloud boxes. This procedure extrapolates the clouds to the 1 K boundary within the box and is necessary in order to include most of the emission from the clouds which comes from regions with $T < T_{\rm min}$—even for the warmest clouds. The 1 K boundaries within the boxes approach, but are not equal to, the true 1 K boundaries which in most cases are blended with nearby emission. Since the cloud velocity boundaries in most cases truncate the cloud-averaged line profiles we have further extended the box in velocity-space by ± 2 km s^{-1}. Use of the 1 K boundary within the above defined cloud boxes typically increases the dispersions in σ_l, σ_b by $\sim 15\%$ and the velocity dispersions by $\sim 50\%$. The final catalog has 273 clouds.

The minimum apparent size criteria above a $T_{\rm min} = 4$ K level means that the peak intensity in the cloud is always greater than 5 K. All but 13 clouds in the catalog have a peak intensity greater than 6 K. These clouds thus represent the warm population described by Solomon, Sanders, and Rivolo (1985) and Rivolo, Solomon, and Sanders (1986).

There is a two-fold (near-far) distance ambiguity for all kinematic distances in the inner Galaxy. We have resolved the ambiguity by utilizing a bootstrap process based on the cloud physical properties measured for a subset of clouds with known distances which serve as *calibrators*. The calibrator clouds include those with small near-far distance ratios (tangent point clouds), and clouds which can be assigned either near or far on the basis of an association with an H II region (Downes *et al.* 1980) for which a distance assignment has been made on the basis of radio absorption line data. These clouds are identified by the flags T = tangent, H = H II region in column (15) of Table 1.

Near or far distances to all noncalibrator clouds were assigned using three criteria: (1) choosing the distance with the better fit to the size–line width relation, discussed in the next section, (2) choosing the near side if the far distance places the cloud more than 150 pc out of the plane, and (3) choosing near or far based on the fit for the scale height of the emission in the longitude and velocity range of the cloud. The third method utilizes the well-determined value for the half-width at half-maximum of the molecular layer of 60 pc (see, e.g., Sanders, Solomon, and Scoville 1984). The details of these methods are presented elsewhere (Solomon *et al.* 1986). The flags in column (15) of Table 1 reflect these methods: V = velocity line width–size relation, Z = height from disk, G = scale height.

III. EMPIRICAL RESULTS

a) Size–Line Width and Mass-Luminosity Laws

For each cloud we define a size parameter S given by

$$S = D \tan\left(\sqrt{\sigma_l \sigma_b}\right),$$

where D is the distance to a cloud. For the calibrators we find a well-defined relationship between the cloud size and the velocity line width. Figure 1 shows the data for all clouds in Table 1 with the calibrators shown as solid symbols. A linear least-squares regression to the logs using only the calibrators leads to the result

$$\sigma_v = 1.0 \pm 0.1 S^{0.5 \pm 0.05}\ (\text{km s}^{-1}), \qquad (1)$$

where S is in parsecs. The dispersion in $\log(\sigma_v)$ is ± 0.11 corre-

TABLE 1

GALACTIC FIRST QUADRANT MOLECULAR CLOUD CATALOG

(1) No.	(2) $T_{min}-I$ (K)	(3) ℓ_p (Deg.)	(4) b_p (Deg.)	(5) v_p (km·s^{-1})	(6) T_p (K)	(7) R (kpc)	(8) D (kpc)	(9) z (pc)	(10) σ_ℓ (Deg.)	(11) σ_b (Deg.)	(12) σ_v (km·s^{-1})	(13) $L_{CO}/10^4$ (K·km·s^{-1}·pc^2)	(14) $M_{VT}/10^4$ ($M_\odot$)	(15) Flag
1	4–3	8.00	−0.50	128.	5.7	1.4	10.1	−89.	0.06	0.07	4.4	7.27	44.4	T
2	5–3	8.20	0.20	20.	10.2	6.2	15.9	56.	0.17	0.21	4.1	140.2	176.3	F,V
3	4–4	8.30	0.00	3.	5.7	4.0	6.2	0.	0.40	0.11	3.8	22.6	65.4	X
4	4–5	8.30	−0.10	48.	8.2	3.6	13.2	−23.	0.05	0.05	2.2	5.02	11.1	F,U
5	5–6	8.40	−0.30	37.	17.0	4.4	5.7	−30.	0.32	0.15	3.9	23.3	66.5	N,H
6	5–4	8.50	−1.00	16.	10.5	6.9	3.2	−55.	0.25	0.25	3.5	10.6	33.7	N,V
7	5–2	8.30	−0.30	16.	6.7	6.8	3.2	−17.	0.16	0.15	2.4	2.81	10.0	N,V
8	4–6	8.70	0.60	22.	7.8	6.1	4.0	42.	0.08	0.09	1.9	0.86	4.2	N,V
9	4–8	8.90	−0.50	12.	5.4	4.0	6.3	−21.	0.04	0.04	3.1	0.94	8.4	X
10	4–11	9.30	0.70	15.	6.6	7.3	2.8	34.	0.03	0.11	2.0	0.20	2.2	N,V
11	4–10	9.30	0.00	31.	7.5	5.3	4.8	0.	0.08	0.08	2.4	1.56	7.8	N,V
12	4–16	9.60	0.80	26.	6.5	5.9	4.2	59.	0.19	0.11	4.4	5.39	41.0	N,V
13	6–14	9.80	−0.75	28.	8.7	5.7	4.4	−57.	0.05	0.10	3.4	1.83	12.4	N,Z
14	6–15	10.00	−0.04	32.	9.7	5.4	4.7	−33.	0.10	0.07	3.1	1.83	13.3	N,V
15	5–15	10.20	−0.30	8.	10.9	3.8	6.5	−34.	0.16	0.11	5.0	18.8	75.1	X
16	5–17	10.60	−0.40	−2.	16.8	3.8	6.5	−45.	0.17	0.11	3.0	10.4	27.9	X
17	5–21	10.80	−0.80	29.	8.1	5.9	4.2	−59.	0.16	0.10	2.9	3.80	15.6	N,V
18	4–21	11.10	−0.40	−2.	12.9	4.0	6.3	−44.	0.10	0.08	3.1	4.55	18.9	X
19	5–18	11.10	−0.50	34.	7.6	5.5	4.8	−42.	0.30	0.33	4.8	57.8	121.3	F,G
20	4–22	11.40	−0.30	49.	6.0	4.5	6.1	−32.	0.09	0.07	2.1	1.79	7.4	N,G
21	5–24	11.60	−0.40	32.	6.3	5.8	4.3	−30.	0.06	0.10	2.8	1.67	9.1	N,V
22	4–26	11.70	−0.30	47.	6.7	4.7	5.6	−29.	0.05	0.06	2.8	1.23	8.3	N,V
23	4–25	11.90	0.80	26.	10.5	6.5	3.6	51.	0.13	0.13	2.4	2.24	9.5	N,Z
24	4–27	11.90	−0.10	42.	5.9	5.1	14.4	−25.	0.07	0.04	3.4	8.46	30.8	F,G
25	5–27	12.00	−0.60	35.	7.1	5.7	4.5	−47.	0.10	0.11	2.6	2.95	11.1	N,V
26	4–31	12.20	−0.10	23.	10.0	6.9	16.3	−28.	0.04	0.04	3.9	8.30	34.6	F,H
27	4–33	12.40	−0.70	25.	6.2	6.7	3.4	−42.	0.05	0.04	2.6	0.32	3.6	N,Z
28	5–29	12.70	0.70	18.	16.1	7.5	2.5	31.	0.23	0.19	2.3	2.81	9.8	N,Z
29	4–36	12.70	−0.10	56.	9.7	4.4	13.6	−24.	0.04	0.05	2.2	4.57	10.2	F,H
30	6–30	12.80	−0.20	32.	22.5	6.1	4.1	−14.	0.29	0.16	6.8	27.8	140.6	N,H
31	5–33	12.90	0.50	35.	8.2	5.9	4.3	38.	0.08	0.06	2.5	1.05	6.5	N,Z
32	4–35	13.00	0.40	32.	9.0	6.2	4.0	28.	0.20	0.13	3.3	3.53	24.5	N,V
33	6–32	13.00	−0.10	47.	10.5	5.0	5.3	−9.	0.17	0.12	4.4	14.0	50.8	N;H
34	4–40	13.70	−0.10	48.	7.5	5.1	5.2	−9.	0.10	0.10	3.2	3.16	18.6	N,V
35	4–43	13.90	0.90	27.	5.2	6.8	3.3	53.	0.10	0.10	3.2	1.32	12.0	N,Z
36	4–42	13.90	0.30	49.	9.0	5.1	5.2	27.	0.12	0.12	3.0	4.72	19.7	N,V
37	4–44	14.00	−0.10	26.	5.7	6.9	3.2	−6.	0.10	0.08	2.3	0.76	5.3	N,V
38	6–33	14.00	−0.60	18.	15.3	7.7	2.4	−25.	0.49	0.33	4.8	19.5	76.2	N,V
39	6–35	14.20	−0.20	39.	15.5	5.8	4.4	−15.	0.36	0.18	4.2	29.7	68.8	N,V
40	4–47	14.60	−0.60	37.	6.6	6.1	4.2	−43.	0.09	0.11	2.3	1.79	7.6	N,Z
41	6–37	15.00	−0.70	20.	42.6	7.7	2.5	−30.	0.16	0.09	3.0	2.51	9.2	N,H
42	5–40	15.00	0.00	25.	8.1	7.2	3.0	0.	0.08	0.04	2.2	0.35	2.8	N,V
43	4–51	15.10	0.90	43.	9.5	5.7	4.6	71.	0.08	0.04	1.6	0.48	2.3	N,Z
44	4–50	15.30	0.00	32.	6.7	6.6	3.6	0.	0.13	0.13	2.3	1.81	8.6	N,V
45	4–57	15.70	−0.20	57.	6.9	5.0	5.4	−19.	0.09	0.08	2.2	1.32	7.8	N,V
46	4–56	15.90	−0.60	19.	12.7	7.9	2.2	−23.	0.27	0.13	2.5	1.60	9.1	N,Z
47	4–60	15.90	0.30	19.	6.8	7.9	2.2	12.	0.15	0.09	1.9	0.42	3.3	N,V
48	4–58	15.90	−1.00	58.	5.1	5.0	5.5	−95.	0.07	0.05	1.5	0.73	2.5	N,Z
49	4–62	16.20	−0.80	56.	6.0	5.1	5.3	−74.	0.03	0.04	1.8	0.32	2.1	N,Z
50	5–45	15.80	−0.60	48.	7.1	5.5	4.8	−51.	0.08	0.08	2.7	1.83	9.8	N,V
51	5–48	16.25	−0.05	48.	10.0	5.6	14.5	−13.	0.07	0.07	2.9	14.3	29.7	F,G
52	5–50	16.70	−0.45	43.	9.9	6.0	4.3	−34.	0.14	0.15	3.2	6.60	22.2	N,G
53	4–63	16.30	−0.40	19.	8.5	7.9	2.2	−15.	0.03	0.07	1.7	0.08	1.0	N,V
54	4–61	16.30	0.40	28.	10.0	7.1	3.1	22.	0.09	0.17	2.7	1.61	9.7	N,G
55	4–64	16.50	0.40	38.	10.0	6.3	3.9	27.	0.11	0.22	5.4	5.36	62.1	N,G

TABLE 1—*Continued*

(1)	(2)	(3)	(4)	(5)	(6)	(7)	(8)	(9)	(10)	(11)	(12)	(13)	(14)	(15)
No.	T_{min}–I	ℓ_p	b_p	v_p	T_p	R	D	z	σ_ℓ	σ_b	σ_v	$L_{CO}/10^4$	$M_{VT}/10^4$	Flag
	(K)	(Deg.)	(Deg.)	(km·s^{-1})	(K)	(kpc)	(kpc)	(pc)	(Deg.)	(Deg.)	(km·s^{-1})	(K·km·s^{-1}·pc^2)	($M_\odot$)	
56	4–67	16.65	–0.05	59.	8.7	5.1	5.4	–5.	0.17	0.09	3.2	4.98	23.9	N,V
57	5–55	16.80	0.10	30.	12.5	7.0	15.9	28.	0.08	0.09	3.3	28.4	51.4	F,V
58	5–54	16.90	0.30	24.	18.0	7.5	2.6	14.	0.22	0.42	4.1	9.73	46.8	N,H
59	4–71	17.20	–0.20	43.	13.0	6.1	14.9	–52.	0.18	0.10	5.8	91.0	234.2	F,V
60	4–74	17.30	–0.90	46.	7.9	5.9	4.4	–70.	0.04	0.06	2.6	0.53	5.1	N,Z
61	5–59	17.70	0.30	22.	8.2	7.8	2.4	12.	0.15	0.09	2.6	0.99	6.5	N,G
62	4–78	17.70	0.10	41.	7.0	6.3	15.1	26.	0.04	0.04	3.4	5.10	24.3	F,V
63	6–56	18.15	–0.30	54.	25.3	5.6	4.9	–25.	0.25	0.18	5.7	24.5	117.0	N,V
64	6–61	18.85	0.05	50.	11.7	5.9	14.4	13.	0.11	0.09	3.2	33.0	51.2	F,G
65	4–82	18.65	0.30	21.	7.1	8.0	16.8	88.	0.09	0.04	3.5	6.35	43.0	F,V
66	5–63	18.85	–0.50	66.	17.9	5.1	5.6	–48.	0.31	0.25	7.5	57.6	302.8	N,H
67	4–86	19.20	–0.30	33.	6.4	7.1	15.7	–82.	0.10	0.09	4.2	27.2	91.6	F,V
68	5–68	19.25	0.05	26.	8.0	7.6	2.6	2.	0.11	0.08	2.6	0.77	5.7	N,V
69	4–88	19.55	0.25	5.	7.1	0.0	0.5	2.	0.11	0.11	1.1	0.01	0.3	N,V
70	4–91	19.60	–0.05	58.	17.8	5.6	4.9	–4.	0.08	0.06	3.1	1.37	11.5	N,V
71	4–89	19.65	–0.65	55.	6.3	5.8	4.8	–54.	0.07	0.08	3.1	1.46	11.9	N,V
72	4–92	19.70	0.10	26.	7.0	7.7	16.3	28.	0.10	0.08	3.3	21.8	55.3	F,V
73	4–95	19.75	–0.65	24.	10.2	7.8	2.4	–27.	0.08	0.06	1.6	0.18	1.5	N,V
74	4–94	19.80	–0.45	69.	10.4	5.1	5.6	–44.	0.16	0.26	4.9	15.3	95.7	N,V
75	4–90	19.90	–0.55	44.	17.8	6.4	4.0	–38.	0.23	0.18	4.3	11.1	51.8	N,U
76	4–97	20.40	0.60	7.	5.2	9.3	0.7	8.	0.11	0.20	0.9	0.04	0.3	N,V
77	4–99	20.55	–0.45	67.	8.7	5.3	13.3	–105.	0.08	0.10	3.9	10.8	63.1	F,V
78	4–101	20.70	–0.30	63.	14.4	5.5	13.6	–71.	0.07	0.05	3.0	7.27	25.2	F,G
79	4–104	20.75	–0.10	59.	15.9	5.7	13.8	–24.	0.08	0.06	3.7	16.8	45.7	F,H
80	4–102	20.75	0.10	77.	6.5	4.9	6.0	10.	0.09	0.11	3.5	3.16	25.4	N,V
81	4–103	20.85	0.00	30.	6.7	7.5	15.9	0.	0.11	0.09	4.5	26.2	111.8	F,V
82	4–108	20.90	–0.30	68.	5.1	5.3	5.4	–28.	0.11	0.09	3.2	3.16	19.3	N,V
83	4–98	21.35	0.35	8.	7.3	9.3	0.8	5.	0.42	0.23	1.9	0.30	3.1	N,V
84	5–84	21.40	–0.65	55.	10.0	6.0	4.6	–52.	0.30	0.11	3.1	8.75	27.7	N,Z
85	4–113	21.75	0.00	67.	9.7	5.4	5.3	0.	0.16	0.09	4.4	4.62	42.8	N,V
86	4–110	21.40	0.00	75.	10.0	5.1	12.8	0.	0.11	0.07	3.6	15.3	50.8	F,V
87	4–116	21.50	0.25	77.	7.4	5.0	5.9	26.	0.05	0.04	2.3	0.55	4.9	N,V
88	4–118	21.90	–0.35	82.	10.5	4.8	12.4	–76.	0.12	0.14	4.7	40.9	123.5	F,V
89	4–122	22.05	0.20	50.	10.2	6.3	4.2	14.	0.19	0.19	3.8	7.09	39.7	N,G
90	5–93	22.35	0.10	85.	9.7	4.8	12.2	21.	0.04	0.07	3.0	7.17	20.2	F,?
91	5–94	22.40	0.30	84.	15.0	4.8	12.2	64.	0.06	0.04	2.2	5.30	10.1	F,?
92	5–96	22.55	–0.05	115.	6.5	3.9	8.5	–7.	0.04	0.04	3.2	2.32	12.2	T
93	7–82	22.55	–0.20	77.	10.2	5.1	12.6	–44.	0.05	0.02	3.0	6.48	12.5	F,U
94	5–98	22.75	–0.25	109.	7.7	4.1	9.2	–34.	0.06	0.05	3.1	4.03	16.9	T
95	4–130	22.80	0.40	92.	7.2	4.6	11.7	82.	0.05	0.07	3.9	9.05	36.7	F,V
96	4–129	22.85	0.40	114.	7.3	4.0	8.4	59.	0.06	0.00	2.7	0.81	9.1	T
97	7–85	23.00	–0.40	74.	13.5	5.3	12.8	–89.	0.29	0.18	7.6	290.1	588.6	F,H
98	6–88	23.00	0.00	81.	8.7	5.0	12.4	0.	0.09	0.07	5.0	20.2	85.6	F,V
99	4–131	23.10	0.60	38.	12.0	7.2	3.2	34.	0.08	0.11	1.4	0.33	2.1	N,V
100	7–94	23.40	–0.25	102.	13.4	4.4	11.0	–48.	0.08	0.07	4.9	25.8	68.9	T,H
101	5–106	23.50	–0.40	73.	7.1	5.4	5.5	–38.	0.09	0.06	3.1	2.18	13.6	N,V
102	7–95	23.55	0.20	82.	12.0	5.1	12.3	43.	0.09	0.08	4.8	28.0	83.7	F,V
103	4–133	23.70	0.50	82.	8.8	5.1	6.1	53.	0.08	0.04	2.4	0.97	6.9	N,V
104	4–132	23.80	0.55	10.	5.3	9.2	0.9	9.	0.17	0.15	1.5	0.11	1.1	N,Z
105	6–100	23.95	0.15	79.	15.3	5.2	5.8	0.	0.06	0.04	2.9	1.50	8.4	N,V
106	5–115	24.20	–0.05	88.	8.6	4.9	11.9	–10.	0.09	0.05	3.0	9.07	24.9	F,H
107	4–141	24.45	–0.80	56.	5.1	6.3	4.3	–61.	0.04	0.05	2.9	0.48	5.7	N,Z
108	6–102	24.45	0.25	120.	16.5	4.1	9.1	40.	0.22	0.18	6.6	109.5	274.9	T
109	4–143	24.50	0.20	38.	8.5	7.3	15.1	53.	0.05	0.07	2.9	7.82	26.2	F,G
110	6–109	24.40	–0.25	60.	7.5	6.1	13.6	–59.	0.05	0.05	3.5	11.1	29.0	F,V

TABLE 1—*Continued*

(1) No.	(2) $T_{min}-I$ (K)	(3) ℓ_p (Deg.)	(4) b_p (Deg.)	(5) v_p (km·s^{-1})	(6) T_p (K)	(7) R (kpc)	(8) D (kpc)	(9) z (pc)	(10) σ_ℓ (Deg.)	(11) σ_b (Deg.)	(12) σ_v (km·s^{-1})	(13) $L_{CO}/10^4$ (K·km·s^{-1}·pc^2)	(14) $M_{VT}/10^4$ ($M_\odot$)	(15) Flag
111	6–110	24.50	−0.15	44.	11.7	6.9	3.5	−9.	0.08	0.11	3.2	2.15	11.8	N,V
112	6–113	24.45	−0.50	44.	10.7	6.9	3.5	−31.	0.20	0.19	4.2	9.85	42.3	N,V
113	4–138	24.50	−0.70	47.	6.7	6.8	3.7	−46.	0.09	0.08	3.4	1.18	12.8	N,G
114	5–119	24.50	−0.25	101.	17.8	4.5	10.9	−48.	0.09	0.08	5.0	15.7	80.8	F,V
115	5–121	24.55	−0.50	61.	8.2	6.1	4.8	−42.	0.10	0.08	3.4	3.50	17.2	N,U
116	5–124	24.60	−0.15	83.	9.0	5.2	12.1	−32.	0.08	0.07	6.3	21.2	125.5	F,V
117	4–142	24.65	−0.10	114.	5.1	4.2	9.1	−15.	0.08	0.13	3.2	6.34	33.1	T
118	5–130	25.20	0.15	105.	11.2	4.5	9.1	27.	0.12	0.05	4.2	8.59	43.1	T
119	4–145	25.25	0.30	47.	11.2	6.8	14.4	75.	0.08	0.09	4.5	16.1	86.2	F,V
120	4–146	25.55	−0.40	116.	7.6	4.3	9.0	−63.	0.04	0.02	2.6	1.04	6.0	T
121	5–128	25.45	−0.20	65.	12.0	6.0	13.2	−46.	0.12	0.16	4.4	62.0	123.4	F,H
122	5–133	25.65	−0.10	94.	12.8	4.9	11.5	−20.	0.21	0.13	6.0	79.3	238.4	F,G
123	5–138	25.45	−0.20	120.	9.2	4.3	9.0	−32.	0.10	0.04	2.8	3.22	15.6	T
124	4–148	25.80	0.45	48.	6.2	6.8	3.7	29.	0.14	0.20	2.8	3.47	17.0	N,Z
125	5–137	25.80	0.25	109.	9.0	4.4	9.0	43.	0.25	0.09	6.6	34.7	204.9	T
126	4–151	25.90	0.20	69.	5.3	5.9	5.1	18.	0.04	0.06	2.0	0.45	3.5	N,V
127	5–140	25.70	−0.15	109.	6.9	4.4	9.0	−21.	0.13	0.11	3.0	13.3	33.8	T
128	5–142	25.90	−0.15	107.	10.2	4.5	9.0	−27.	0.15	0.11	5.6	27.3	126.3	T
129	4–150	25.95	−0.60	63.	5.8	6.1	4.7	−49.	0.07	0.07	2.1	0.94	5.1	N,V
130	4–153	26.20	0.10	71.	5.9	5.8	5.2	9.	0.09	0.08	2.9	1.73	12.9	N,V
131	4–156	26.35	0.80	47.	6.6	6.9	3.6	51.	0.13	0.05	1.9	0.53	3.7	N,Z
132	4–152	26.50	−0.60	67.	7.8	6.0	4.9	−52.	0.15	0.21	4.3	9.35	56.4	N,G
133	5–146	26.55	−0.30	108.	10.9	4.6	8.9	−42.	0.08	0.04	2.8	3.95	13.8	T
134	4–159	26.60	0.00	26.	7.2	8.2	15.8	0.	0.03	0.11	3.9	18.6	48.1	F,V
135	5–149	26.65	0.00	100.	9.1	0.6	9.6	0.	0.10	0.16	4.3	22.2	78.2	T
136	4–158	26.70	0.50	86.	7.7	5.3	6.2	54.	0.07	0.07	2.0	1.34	6.0	N,V
137	4–162	26.65	0.00	112.	6.4	4.5	8.9	0.	0.06	0.04	2.9	2.39	12.8	T
138	5–154	26.90	0.10	91.	9.6	5.1	6.5	11.	0.12	0.07	3.0	4.44	18.7	N,V
139	4–165	26.95	−0.40	69.	12.5	6.0	5.0	−35.	0.09	0.02	2.2	0.57	3.6	N,V
140	4–160	26.95	−0.10	81.	7.5	5.5	5.8	−10.	0.14	0.08	2.5	2.21	13.4	N,V
141	4–167	27.05	−0.15	101.	7.4	4.8	8.9	−19.	0.06	0.04	2.3	2.15	8.0	T
142	4–170	27.25	0.15	33.	8.5	7.8	15.2	40.	0.09	0.05	4.4	14.8	68.8	F,V
143	4–174	27.30	−0.30	72.	6.5	5.9	5.2	−27.	0.07	0.07	3.2	1.45	13.0	N,V
144	4–173	27.35	−0.15	93.	10.5	5.1	6.6	−17.	0.06	0.04	2.3	1.80	6.0	N,V
145	4–176	27.50	0.20	36.	10.2	7.6	15.0	52.	0.04	0.04	2.9	4.61	17.5	F,V
146	6–155	27.50	0.15	95.	8.8	5.1	10.9	29.	0.08	0.07	4.7	16.7	63.0	F,V
147	4–175	27.65	0.10	83.	8.0	5.5	5.9	10.	0.11	0.07	3.5	3.21	22.2	N,V
148	6–157	27.75	0.10	101.	8.7	4.9	8.9	13.	0.13	0.12	3.3	14.1	41.9	T
149	6–159	28.20	−0.05	95.	9.3	5.1	10.8	−9.	0.04	0.10	5.5	15.0	72.0	F,V
150	4–178	28.30	−0.35	47.	7.6	7.1	3.5	−21.	0.21	0.09	3.2	1.86	17.2	N,V
151	6–158	28.30	−0.10	81.	13.0	5.6	5.8	−10.	0.15	0.14	4.1	18.6	49.1	N,G
152	6–165	28.60	0.05	100.	10.0	5.0	8.8	9.	0.09	0.09	5.2	14.1	74.5	T,H
153	5–174	28.80	0.20	79.	7.2	5.8	11.9	42.	0.06	0.04	3.5	6.81	24.9	F,V
154	6–162	28.85	−0.25	88.	15.8	5.4	6.3	−27.	0.12	0.07	6.0	9.44	72.2	N,G
155	6–168	29.10	−0.30	94.	11.0	5.2	7.1	−37.	0.25	0.11	4.0	22.3	65.6	N,V
156	4–187	28.95	−0.65	51.	12.0	7.0	3.8	−43.	0.09	0.08	2.5	0.76	6.9	N,Z
157	6–171	29.35	−0.45	77.	10.5	5.9	5.4	−43.	0.19	0.12	5.3	14.1	80.1	N,G
158	6–169	29.00	0.05	98.	10.9	5.1	8.8	6.	0.19	0.10	3.7	25.5	57.5	T
159	4–189	29.35	−0.55	64.	6.3	6.4	4.6	−44.	0.11	0.10	3.3	2.57	18.3	N,V
160	6–174	29.55	0.20	79.	11.0	5.8	5.6	20.	0.14	0.11	3.0	8.74	21.9	N,G
161	4–191	29.60	−0.60	75.	7.9	6.0	12.1	−126.	0.11	0.13	4.4	27.4	97.2	F,V
162	6–179	29.85	−0.05	100.	20.5	5.1	8.7	−6.	0.15	0.10	5.2	35.0	100.1	T,H
163	4–194	29.90	0.10	40.	6.6	7.6	14.4	25.	0.05	0.02	3.3	4.40	17.3	F,V
164	4–193	29.90	−0.80	83.	7.0	5.7	5.9	−82.	0.12	0.05	2.3	1.75	8.4	N,V
165	4–199	30.40	0.45	45.	10.0	7.4	3.3	26.	0.04	0.07	1.6	0.20	1.5	N,V

TABLE 1—*Continued*

(1) No.	(2) T_{min}–I (K)	(3) ℓ_p (Deg.)	(4) b_p (Deg.)	(5) v_p (km·s^{-1})	(6) T_p (K)	(7) R (kpc)	(8) D (kpc)	(9) z (pc)	(10) σ_ℓ (Deg.)	(11) σ_b (Deg.)	(12) σ_v (km·s^{-1})	(13) $L_{CO}/10^4$ (K·km·s^{-1}·pc^2)	(14) $M_{VT}/10^4$ ($M_\odot$)	(15) Flag
166	4–198	30.50	–0.65	12.	15.3	9.2	0.9	–10.	0.08	0.14	1.4	0.04	0.7	N,V
167	5–186	30.55	0.35	95.	9.9	5.3	8.6	63.	0.08	0.10	4.2	7.94	47.3	T
168	4–197	30.60	–0.05	43.	7.2	7.5	14.1	–12.	0.14	0.09	4.7	32.1	121.7	F,G
169	6–191	30.60	–0.45	94.	11.2	5.4	10.3	–81.	0.04	0.06	3.9	7.57	26.8	F,V
170	6–188	30.60	–0.10	115.	8.1	5.1	8.6	–15.	0.09	0.07	3.4	5.69	27.5	T
171	7–174	30.80	–0.05	92.	16.1	5.4	6.8	–6.	0.20	0.24	5.2	76.6	140.4	N,H
172	4–201	30.85	–0.15	53.	11.5	7.0	3.9	–10.	0.07	0.09	2.6	0.82	7.4	N,V
173	5–193	30.90	–0.60	102.	7.2	5.2	8.6	–96.	0.05	0.02	3.3	1.31	10.3	T
174	4–204	30.95	0.10	40.	7.7	7.6	14.2	25.	0.08	0.10	4.2	23.7	78.2	F,G
175	6–196	30.95	0.40	77.	8.4	6.0	5.5	38.	0.09	0.07	3.0	2.97	13.6	N,G
176	7–173	30.30	–0.25	105.	14.9	5.2	8.6	–36.	0.07	0.19	4.0	26.5	55.5	T,H
177	6–199	31.30	0.00	79.	7.7	6.0	5.6	0.	0.08	0.10	3.4	4.19	20.2	N,V
178	4–207	31.40	0.00	39.	8.8	7.7	14.2	0.	0.19	0.11	4.5	51.4	145.2	F,G
179	5–198	31.40	–0.25	88.	8.5	5.7	10.7	–47.	0.05	0.04	2.9	3.02	14.1	F,H
180	6–204	31.45	0.05	104.	8.7	5.2	8.5	7.	0.10	0.08	4.2	10.2	46.9	T
181	4–215	31.95	–0.30	97.	6.2	5.4	8.5	–38.	0.07	0.07	3.5	4.93	25.4	T
182	5–200	32.00	0.00	98.	10.5	5.4	8.5	0.	0.22	0.09	3.0	16.6	37.3	T
183	4–217	32.45	0.20	51.	6.4	7.2	13.3	46.	0.04	0.04	2.6	3.43	12.5	F,G
184	4–218	32.60	–0.25	90.	10.5	5.7	10.3	–45.	0.17	0.14	7.9	56.5	344.2	F,V
185	4–223	33.35	–0.55	92.	6.6	5.7	8.4	0.	0.07	0.10	2.2	3.65	11.8	T
186	4–220	33.40	0.00	75.	13.3	6.3	11.4	0.	0.16	0.07	4.3	16.7	77.6	F,G
187	4–222	33.45	–0.10	87.	7.2	5.9	10.3	–18.	0.15	0.10	3.9	19.1	67.1	F,G
188	4–225	33.80	–0.20	48.	7.1	7.4	13.2	–47.	0.11	0.07	3.7	13.8	55.3	F,G
189	4–226	33.65	0.20	42.	6.0	7.7	13.6	35.	0.06	0.05	2.8	4.89	20.4	F,G
190	4–227	33.85	0.00	89.	6.4	5.8	10.0	0.	0.10	0.05	3.6	5.73	32.0	F,G
191	4–221	33.90	0.10	106.	9.5	5.6	8.3	14.	0.20	0.08	4.2	18.2	64.5	T
192	4–233	34.15	–0.10	89.	6.8	5.8	8.3	–17.	0.06	0.10	3.2	4.04	22.9	T
193	4–228	34.25	0.10	53.	8.2	7.2	3.7	7.	0.19	0.15	4.6	5.09	46.4	N,H
194	4–229	34.35	–0.85	13.	5.3	9.2	0.9	–14.	0.22	0.21	1.5	0.25	1.6	N,Z
195	4–235	34.40	–0.20	53.	6.4	7.2	3.7	–13.	0.10	0.05	2.6	0.67	6.2	N,G
196	4–239	34.80	–0.15	76.	6.7	6.3	5.6	–15.	0.10	0.10	3.7	3.89	26.9	N,V
197	4–232	34.65	–0.80	55.	7.1	7.2	3.9	–54.	0.22	0.14	3.0	3.75	21.2	N,G
198	5–222	35.05	0.30	51.	13.8	7.4	3.6	19.	0.19	0.12	3.1	4.41	18.1	N,G
199	5–223	35.15	–0.75	35.	22.3	7.5	3.3	–43.	0.15	0.12	3.1	3.08	14.8	N,Z
200	5–220	34.70	–0.70	46.	10.0	7.5	3.3	–40.	0.26	0.38	6.7	23.0	162.3	N,Z
201	4–240	35.20	–0.10	13.	6.2	9.3	0.9	–2.	0.15	0.43	1.7	0.38	2.4	N,G
202	4–241	35.75	0.15	82.	8.5	6.2	10.2	27.	0.20	0.08	4.2	27.3	79.2	F,V
203	4–244	35.80	–0.20	29.	7.7	8.4	2.0	–7.	0.36	0.14	1.8	0.77	5.2	N,V
204	5–230	35.95	–0.50	58.	10.5	7.1	4.1	–36.	0.05	0.06	2.4	0.62	4.5	N,V
205	4–248	36.10	0.65	77.	11.5	6.4	5.6	63.	0.17	0.22	4.3	10.1	69.7	N,G
206	5–234	36.40	–0.10	52.	8.9	7.4	3.6	–6.	0.23	0.12	3.6	6.06	27.3	N,V
207	5–237	36.50	–0.15	77.	9.9	6.4	5.9	–15.	0.17	0.14	3.2	10.7	32.3	N,V
208	5–238	36.90	–0.05	80.	8.9	6.5	5.9	–5.	0.08	0.08	2.8	3.65	12.9	N,V
209	4–254	37.35	0.25	88.	6.4	6.1	8.6	38.	0.13	0.15	3.8	19.9	60.7	T
210	4–258	37.45	0.10	41.	9.2	7.9	3.0	6.	0.08	0.08	2.5	0.40	5.2	N,V
211	4–261	37.75	–0.20	60.	8.0	7.1	11.6	–40.	0.05	0.08	5.2	13.7	68.9	F,H
212	4–265	38.25	–0.15	65.	7.3	7.0	11.1	–29.	0.06	0.02	3.9	3.27	20.3	F,G
213	4–269	38.95	–0.45	42.	16.3	7.9	2.9	–23.	0.12	0.14	3.6	1.63	17.2	N,G
214	4–272	39.85	–0.20	57.	8.1	7.4	11.3	–39.	0.42	0.19	6.3	171.8	441.5	F,G
215	4–276	40.30	–0.45	74.	7.8	6.8	5.7	–45.	0.08	0.07	2.8	1.47	11.6	N,V
216	4–281	41.00	–0.20	38.	6.0	8.2	2.7	–9.	0.12	0.20	2.7	1.61	10.4	N,V
217	4–279	41.15	–0.20	60.	11.0	7.3	10.7	–37.	0.10	0.20	6.7	46.4	236.7	F,G
218	4–284	41.90	–0.40	59.	8.2	7.4	10.6	–74.	0.09	0.08	3.6	8.43	40.5	F,G
219	4–288	42.35	–0.05	58.	6.7	7.4	10.5	–9.	0.06	0.08	4.0	8.02	40.6	F,G
220	4–286	42.15	–0.60	67.	10.7	7.1	5.4	–57.	0.07	0.16	3.1	5.03	19.2	N,U

TABLE 1—*Continued*

(1) No.	(2) T_{min}–I (K)	(3) ℓ_p (Deg.)	(4) b_p (Deg.)	(5) v_p (km·s^{-1})	(6) T_p (K)	(7) R (kpc)	(8) D (kpc)	(9) z (pc)	(10) σ_ℓ (Deg.)	(11) σ_b (Deg.)	(12) σ_v (km·s^{-1})	(13) $L_{CO}/10^4$ (K·km·s^{-1}·pc^2)	(14) $M_{VT}/10^4$ ($M_\odot$)	(15) Flag
221	4–289	42.75	−0.35	59.	6.0	7.4	4.6	−28.	0.16	0.11	3.6	3.98	27.3	N,U
222	4–292	43.10	0.05	12.	8.7	9.4	13.8	12.	0.05	0.05	4.9	10.2	57.6	F,V
223	4–291	43.20	−0.50	57.	8.2	7.5	4.4	−38.	0.07	0.05	2.5	0.75	5.7	N,U
224	4–297	44.35	−0.20	64.	7.4	7.3	9.2	−32.	0.16	0.20	5.2	42.6	155.6	F,V
225	4–300	45.45	0.05	58.	10.5	7.6	9.5	8.	0.25	0.12	4.8	28.9	132.2	F,H
226	4–304	46.30	−0.20	59.	7.7	7.5	9.1	−32.	0.14	0.02	3.5	4.65	20.5	F,G
227	4–305	47.05	0.25	55.	9.2	7.7	9.3	40.	0.14	0.04	2.5	4.18	15.1	F,G
228	4–306	47.40	−1.00	7.	5.3	9.7	0.5	−9.	0.11	0.04	1.3	0.01	0.2	N,V
229	4–307	47.55	−0.55	59.	5.6	7.6	8.5	−82.	0.09	0.06	2.1	2.47	9.6	F,G
230	4–313	48.60	0.25	10.	7.0	9.6	12.5	55.	0.06	0.04	3.0	3.65	19.2	F,V
231	4–312	48.60	0.00	20.	13.5	9.1	11.8	0.	0.06	0.06	2.6	6.34	16.7	F,H
232	4–311	48.85	0.15	51.	8.0	7.9	6.6	15.	0.14	0.11	2.6	3.87	19.3	T
233	4–314	49.50	−0.40	57.	24.1	7.7	6.6	−47.	0.28	0.24	7.4	66.5	326.5	T,H
234	4–317	49.75	−0.55	68.	10.7	7.6	6.5	−62.	0.07	0.06	2.5	1.54	9.1	T
235	3–281	50.05	0.60	−2.	10.5	10.1	13.0	136.	0.08	0.08	2.5	11.2	22.7	F,G
236	3–290	50.85	0.25	43.	7.0	8.3	3.6	16.	0.07	0.08	2.7	0.57	6.8	N,V
237	3–294	51.35	−0.05	54.	11.5	7.9	6.3	−5.	0.19	0.12	3.3	7.13	35.8	T
238	4–326	52.30	−0.05	52.	5.7	8.0	6.1	0.	0.06	0.06	2.3	0.73	6.8	T
239	3–301	52.55	−0.95	64.	13.4	7.9	6.1	−101.	0.27	0.12	3.4	9.72	44.1	T
240	4–333	53.15	−0.25	61.	10.7	8.0	6.0	0.	0.07	0.04	2.6	1.17	7.5	T
241	3–307	53.55	0.05	23.	17.8	9.1	1.8	2.	0.36	0.28	1.8	1.11	6.3	N,V
242	3–318	54.10	−0.05	40.	14.2	8.4	8.2	−7.	0.06	0.05	2.6	2.19	10.6	F,G
243	3–321	54.65	0.80	31.	6.2	8.8	9.0	125.	0.10	0.12	3.1	6.71	32.9	F,V
244	3–323	55.30	0.20	30.	7.2	8.8	9.0	31.	0.10	0.10	3.1	7.26	30.1	F,V
245	4–345	59.30	−0.20	28.	11.7	8.9	2.7	−9.	0.11	0.10	1.9	0.61	3.5	N,H
246	4–347	60.00	0.10	22.	11.9	9.2	8.0	14.	0.18	0.15	3.3	11.0	49.8	F,G
247	3–335	60.90	−0.10	23.	19.9	9.1	7.5	−13.	0.05	0.05	1.3	1.38	2.2	F,G
248	3–337	61.50	0.10	22.	15.5	9.2	7.4	13.	0.09	0.07	1.8	3.29	6.6	F,G
249	3–339	63.10	0.40	20.	11.9	9.3	7.0	49.	0.07	0.05	1.8	2.12	4.7	F,G
250	3–346	70.90	0.70	12.	5.7	9.6	1.8	21.	0.07	0.07	1.6	0.11	1.1	N,G
251	3–345	71.10	−0.40	10.	7.0	9.6	1.4	−10.	0.23	0.21	1.9	0.52	3.9	N,V
252	3–354	76.20	0.10	−2.	16.3	10.1	5.1	9.	0.22	0.19	2.7	7.20	26.5	F,H
253	3–357	76.30	−0.70	−1.	16.0	10.0	4.9	−60.	0.10	0.23	2.5	4.32	16.2	F,H
254	3–359	77.20	0.70	2.	5.8	10.0	4.1	4.	0.36	0.21	3.4	7.57	45.2	F,V
255	3–361	78.00	−0.30	−4.	8.2	10.2	4.8	−25.	0.09	0.15	2.5	1.98	12.1	F,V
256	4–367	78.10	−0.80	0.	10.7	10.0	4.1	0.	0.15	0.13	2.6	2.97	13.6	F,V
257	4–370	78.20	0.10	11.	6.2	9.8	2.0	4.	0.18	0.23	2.9	1.13	12.2	T
258	4–374	78.80	−0.50	−1.	11.5	10.0	4.1	−36.	0.16	0.14	2.8	4.21	16.7	F,V
259	4–377	79.20	0.10	8.	10.0	9.8	1.9	3.	0.10	0.22	2.3	0.64	5.1	T
260	4–379	79.10	1.00	7.	9.7	9.8	1.9	33.	0.12	0.04	1.6	0.07	1.2	T
261	4–384	79.50	1.00	12.	6.4	9.8	1.8	32.	0.03	0.04	2.6	0.07	1.5	T
262	4–381	79.60	−0.60	4.	6.6	9.9	2.5	−26.	0.15	0.14	3.1	1.21	12.2	F,V
263	3–373	80.70	0.70	−1.	9.3	10.0	3.5	42.	0.18	0.12	3.3	1.41	19.3	F,V
264	3–374	80.80	−0.50	−3.	9.0	10.0	3.8	−34.	0.05	0.09	1.3	0.36	1.5	F,V
265	4–391	81.20	1.00	13.	14.0	9.9	1.5	27.	0.14	0.18	4.6	0.90	17.9	T
266	4–394	81.40	0.70	−2.	9.2	10.1	3.5	42.	0.13	0.11	1.9	1.03	5.2	F,V
267	3–377	81.40	0.00	−4.	14.0	10.1	2.0	0.	0.21	0.10	1.8	0.36	3.3	N,H
268	4–395	81.70	0.60	−2.	14.0	10.1	2.0	21.	0.03	0.30	5.7	4.29	21.5	N,H
269	4–396	82.00	−0.40	5.	6.2	9.9	1.4	−10.	0.18	0.18	2.2	0.41	4.2	T
270	3–380	83.30	−0.20	2.	7.4	9.3	1.2	−4.	0.11	0.06	0.9	0.03	0.3	T
271	3–381	83.50	−1.00	2.	5.5	9.9	1.1	−20.	0.15	0.20	1.9	0.20	2.5	T
272	3–383	84.60	0.20	−1.	12.7	10.0	2.0	7.	0.18	0.45	3.5	4.86	23.7	F,V
273	3–387	85.40	0.00	−38.	8.7	11.8	7.1	0.	0.03	0.03	2.2	0.61	3.6	F,V

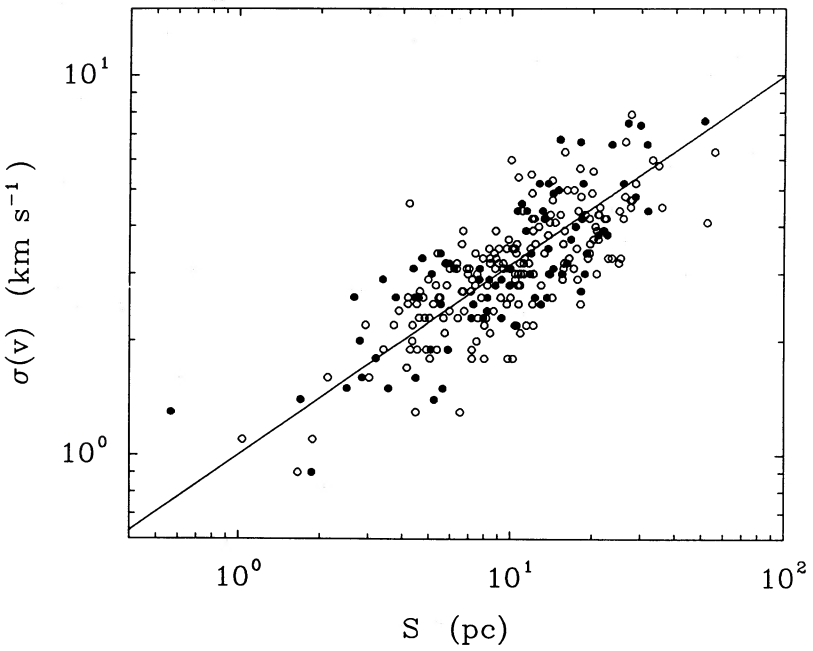

FIG. 1.—Molecular cloud velocity dispersion $\sigma(v)$ as a function of size S (defined in text) for 273 clouds in the Galaxy. The solid circles are calibrator clouds with known distances and the open circles are for clouds with the near-far distance ambiguity resolved by the method discussed in the text. The fitted line is $\sigma(v) = S^{0.5}$ km s^{-1}. For virial equilibrium the 0.5 power law requires clouds of constant average surface density.

sponding to 30% in σ_v. This size–line width relation holds over a factor of 30 in size. Nearly identical fit parameters are achieved using all data points for the fit. The quoted error in the exponent is larger than the formal fit error and represents an estimate of the systematic error based on several fits to the data with varying definitions of cloud boundaries. We note that without the 2 km s^{-1} extrapolation in velocity, the constant in equation (1) is 0.83—a reduction of 17%.

Myers (1983, and references therein) has found a similar relation using 46 small dark clouds with radii less than 2 pc. He finds a very similar exponent (0.52), but his constant of proportionality is smaller by almost a factor of 2. Myers's cloud sizes were defined by peak intensities rather than integrated intensities and thus a direct quantitative comparison is not possible. Larson (1981), from a literature search, suggested that the observed exponent was close to $\frac{1}{3}$ and reflected a Kolmogorov turbulent spectrum. This hypothesis is ruled out by the data presented here. We interpret the size–line width relation as arising from virial equilibrium (Solomon, Scoville, and Sanders 1979; Myers 1983). Previous determinations of the size–line width relation using 80 GMCs (Sanders, Scoville, and Solomon 1985) and 26 GMCs (Dame *et al.* 1986) are consistent with the results presented here, although those data are much less complete and cover a smaller range in size.

Having determined physical sizes for each cloud a virial theorem mass can now be determined from the measured velocity dispersion

$$M_{\rm VT} = 3f_p \frac{S\sigma_v^2}{G} (M_\odot) , \qquad (2)$$

where f_p is a projection factor, and $G = 1/232$ is the Newtonian constant using units of km s^{-1} and parsecs. In applying the virial theorem we are interpreting the CO velocity dispersion as a measure of the internal dynamics of the mass distribution within the clouds. This intepretation is motivated by the observation that the CO line profiles, averaged over a cloud, have Gaussian shapes, even though the emission is known to be optically thick, and that these profiles are very much broader than the thermal line widths (typically a few tenths of km s^{-1}) i.e., the velocity field is highly supersonic. In § IV we present a cloud model which is consistent with the above interpretation.

From relations (1) and (2) it immediately follows that the mean surface density of the clouds is independent of size, and the mean spatial density scales inversely with size. For simplicity we consider spherically symmetric clouds with a power-law density distribution

$$\rho(r) = \rho_1 \left(\frac{R_1}{r}\right)^\alpha \qquad (3)$$

truncated at $r = R_1$. Since we have used rectangular boundaries to compute cloud sizes, we define an *effective radius* such that $\pi R_e^2 = A = \Delta l \Delta b$ where Δl, Δb are the extents of the clouds projected in l and b. From the data we find that on average $\Delta x = 3.4\sigma_x$; thus the effective radius is related to the parameter S by

$$R_e = \frac{3.4}{(\pi)^{1/2}} S .$$

If all clouds have the same density profile, then $\alpha = 1$ and the projection factor is $f_p = 2.9$. We believe that $\alpha = 1$ is close to the real case, since this results in surface density profiles which are similar to those observed. We adopt $\alpha = 1$ henceforth; however, we note that variations in α have little effect on f_p and therefore on derived masses. For example, if $\alpha = 2$ then $f_p = 2.5$. The virial theorem in equation (2) can be rewritten as

$$M = 1040 R_e \tau^2 (M_\odot) .$$

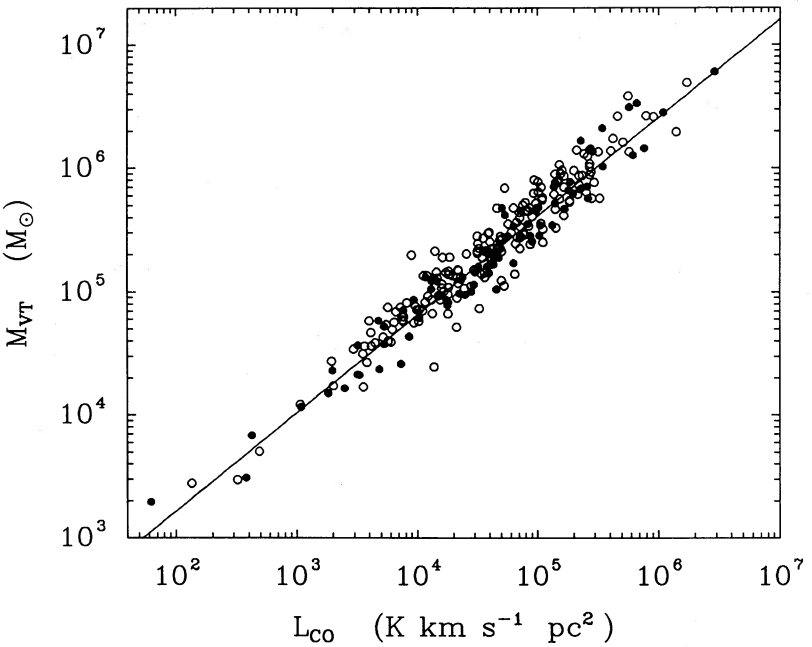

FIG. 2.—The virial mass–CO luminosity relation for molecular clouds. The clouds range in distance from 2 to 15 kpc and in flux over more than two orders of magnitude. The solid circles and open circles are the same as in Fig. 1. The fit is $M_{VT} = 39(L_{CO})^{0.81}\ M_\odot$. For a given CO luminosity the dispersion in virial mass is 0.13 in the log.

Using equations (1) and (2) with $f_p = 2.9$ and $A = 11.6\ S^2$ then yields an average surface density

$$\bar{\Sigma} = 170\ M_\odot\ \mathrm{pc}^{-2} \tag{4}$$

and an average spatial density

$$\bar{\rho} = \frac{134}{R_e}\ M_\odot\ \mathrm{pc}^{-3}\ . \tag{5}$$

Since typical values of R_e range from 6 to 60 pc, the mean molecular hydrogen densities in the clouds are in the approximate range $50 < n(\mathrm{H_2}) < 500\ \mathrm{cm}^{-3}$. Equations 1 and 2 also directly yield a mass–line width relation

$$M = 2000\sigma_v^4\ (M_\odot) \tag{6a}$$

and a mass-radius relation

$$M = 540R_e^2\ (M_\odot)\ . \tag{6b}$$

For each cloud a CO luminosity is obtained directly from the survey data within the boxes circumscribing the cloud boundaries. Explicitly

$$L_{CO} = D^2 \int\int\int T_R^*(l, b, v)dldbdv\ (\mathrm{K\ km\ s^{-1}\ pc^2}) \tag{7}$$

for all $T_R^* > T_{min} = 1$. Figure 2 shows the virial mass as a function of CO luminosity for all clouds with the calibrators shown as filled circles. Again, a least-squares fit to all the data gives essentially the same result as a fit to the calibrators only. The result yields a very tight power law for the mass-luminosity relation over four decades given by

$$M_{VT} = 39(L_{CO})^{0.81\pm0.03}\ (M_\odot) \tag{8}$$

with a dispersion of 0.11 in log (M_{VT}) or 30% in M_{VT}. *This relationship clearly shows that CO luminosity is a good tracer of mass in the inner Galaxy.*

Combining the empirical size–line width and mass-luminosity relations with the virial theorem yields a relation between luminosity and velocity-width analogous to the Tully-Fisher or Faber-Jackson relation for galaxies

$$L_{CO} = 130\sigma_v^5\ (\mathrm{K\ km\ s^{-1}\ pc^2})\ , \tag{9}$$

in agreement with the relation that can be found directly from the data.

The large number statistics of these data allows a reevaluation of the mass spectrum for molecular clouds. Figure 3 shows the mass spectrum of all clouds in Table 1. The differential distribution varies as $dN/dM \propto M^{-3/2}$. This is consistent with previous determinations by Solomon and Sanders (1980),

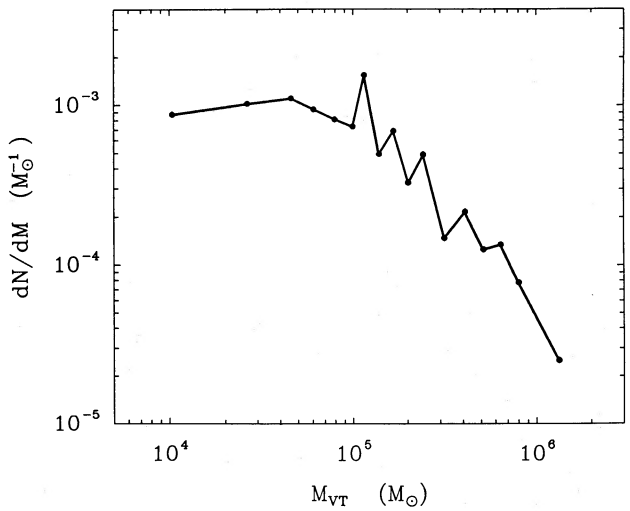

FIG. 3.—The molecular cloud mass spectrum dN/dM. A fit to the data above $M = 7 \times 10^4\ M_\odot$ gives $dN/dM \propto M^{-3/2}$. There are 15 clouds in each bin and the standard deviation is ±24%. The turnover at low mass is due to undercounting of smaller clouds in the more distant parts of the galactic disk.

TABLE 2

CALIBRATION OF CO INTEGRATED INTENSITY WITH H_2 COLUMN DENSITY

Method	Location	$a = \bar{N}(H_2)/\bar{I}_{CO}$ (cm^{-2}/K km s^{-1})	References
$A_V \leq 4$ (in dark clouds)	Local	$2.2(10)^{20}$	Dickman 1975
$A_V \geq 5$	Local	$5.0(10)^{20}$	Liszt 1982
$A_V > 5$	Local	$3.6(10)^{20}$	Sanders, Solomon, and Scoville 1984
γ-rays	Orion	$2.6(10)^{20}$	Bloemen *et al.* 1984
	$5 \leq R \leq 10$ kpc	$1.0(10)^{20}$	Bhat *et al.* 1985
γ-rays	$5 \leq R \leq 10$ kpc	$2.8(10)^{20}$	Bloemen *et al.* 1986
Virial theorem	$4 \leq R \leq 8$ kpc	$3.0(10)^{20}$	This work

Liszt, Xiang, and Burton (1981), and Sanders, Scoville, and Solomon (1985).

The turnover below $M = 5 \times 10^4\ M_\odot$ results from incompleteness in this catalog due to the combination of survey resolution and our strict minimum flux criteria for inclusion in the catalog. The mass fraction of clouds per logarithmic mass interval varies as $M(dN/d \log M) \propto M^{+1/2}$ demonstrating that most of the mass resides in clouds at the high end of the spectrum (Solomon and Sanders 1980).

b) *Mass to CO-Luminosity Calibration*

The observed cloud mass–CO luminosity relation can be translated into a molecular hydrogen column density using the CO integrated intensity averaged over the cloud, $\bar{I}_{CO} = \langle \int T dv \rangle$. The cloud mass and luminosity are then related to the averaged integrated intensity by

$$L_{CO} = A\bar{I}_{CO}$$

$$M = A\bar{N}(H_2)m_{H_2},$$

where $\bar{N}(H_2)$ is the mean H_2 column density in the cloud, and A the area of the cloud projected onto the line of sight. Letting $\bar{N}(H_2) = a\bar{I}_{CO}$ and substituting into the empirical mass-luminosity law (eq. [8]) then yields the values $a = 4.1 \times 10^{20}$ for $M = 10^5\ M_\odot$ and $a = 2.5 \times 10^{20}$ for $M = 10^6\ M_\odot$.

Although the mass is not strictly a linear function of CO luminosity, the conversion factor varies by only a factor of 2 between clouds ranging in mass over a factor of $2^5 = 32$. For the cloud mass distribution observed here the median of the distribution is near $M = 5 \times 10^5\ M_\odot$ which yields $a = 3.0 \times 10^{20}$.

Table 2 presents a summary of conversion factors derived by various methods. The only other technique which has determined the CO luminosity-to-mass conversion factor for giant molecular clouds with $M > 10^5\ M_\odot$ uses the observed γ-ray flux resulting from cosmic-ray interactions with hydrogen molecules. There is excellent agreement between the γ-ray derived conversion factor of Bloemen *et al.* (1986) and that derived here by application of the virial theorem. The conversion factor based on the variation of optical extinction determined along lines of sight with measured ^{12}CO or ^{13}CO integrated intensity also gives good agreement with this work. Bhat *et al.* (1985) have argued for a substantially lower conversion factor for the inner Galaxy scaling from the Bloemen *et al.* (1984) Orion data. Their method, however, is founded on the erroneous assumption that the CO line intensity scales with CO abundance. This assumption is in direct contradiction with the observations, which show that that ^{13}CO emission is typically 1/5 that of ^{12}CO although the abundance ratio is typically 1/90. There is no evidence for a radial decrease in the conversion factor between $R = 10$ and $R = 5$ kpc as suggested by Bhat *et al.* (1984) and Blitz and Shu (1980).

The consistency of results between these independent methods for determining the H_2 mass, demonstrates that the assumption of virial equilibrium in molecular clouds is indeed correct. *Molecular clouds are therefore bound by self-gravity and not by pressure equilibrium with a hot phase of the interstellar medium (ISM).*

The agreement in the conversion factor between very diverse techniques, particularly between the γ-ray results for the inner Galaxy and this work, supports the use of CO emission as a tracer of molecular hydrogen and provides an empirical basis for the determination of the total mass of molecular hydrogen in the inner Galactic disk (see, e.g., Sanders, Solomon, and Scoville 1984 and Table 3).

IV. CONCEPTUAL MODEL

The empirical size–line width relation (eq. [1]) and mass-CO luminosity law (eq. [8]) provide a basis for a simple conceptual model which allows the use of optically thick CO emission as a tracer of mass, primarily molecular hydrogen, in interstellar clouds. Both the existence and the form of the mass-CO luminosity law may be interpreted as a consequence of the internal structure and gravitational equilibrium of giant molecular clouds. We adopt what may be called a "mist" model for the clouds. This model assumes that a cloud consists of a large number of small, optically thick regions (droplets), but with a filling factor at any fixed velocity which is less than 1; a molecular cloud may thus be interpreted as a cluster of separated, discrete particles which is effectively optically thin at each

TABLE 3

TOTAL GALACTIC H_2 MASS FOR $2 < R < 10$ kpc

Reference	M ($10^9\ M_\odot$)	a (cm^{-2}/K km s^{-1})
Scoville and Solomon	1–3	
Gordon and Burton 1976	2.1	
Solomon, Sanders, and Scoville 1979	3.9	5×10^{20}
Thaddeus and Dame 1983	0.7	$(1–2) \times 10^{20}$
Sanders, Solomon, and Scoville 1984	2.6	3.6×10^{20}
Bronfman and Thaddeus 1987	1.3[a]	2.8×10^{20}
This work	2.0[b]	3.0×10^{20}

[a] The difference between this and 2.0 is primarily due to a different weighting used to obtain the radial emissivity and to a 20% lower CO intensity calibration.

[b] The emissivity has been calculated using equal weight per unit of projected face on area for each radial bin.

velocity. The observed line profiles averaged over the cloud have an optically thin appearance in that they have a Gaussian, or near Gaussian, shape. In this model the emission intensity, T_R^*, along any line of sight and velocity v will be proportional to the filling factor of the droplets at v and the kinetic temperature of the droplets T_k. For a Gaussian line profile the average surface brightness of the cloud is $I = (2\pi)^{1/2} T_0 \sigma_v$, where σ_v is the velocity dispersion between the droplets, and T_0 is the peak intensity at the line center averaged over the cloud.

The CO luminosity of a cloud is the product of the surface area ($11.6S^2$) and the surface brightness which is given by

$$L_{CO} = 11.6(2\pi)^{1/2} T_0 \sigma_v S^2 . \quad (10)$$

In the above model the ratio T_0/T_k is the average filling factor of the droplets in the cloud at line center. In contrast, if the clouds were smooth and the emission optically thin, T_0/T_k would represent a measure of the optical depth. Utilizing the size–line width relation in equation (10) then yields

$$L_{CO} = 30 T_0 \sigma_v^5 \ (M_\odot) . \quad (11)$$

Combining the above equation with the virial theorem (eq. [2]) and utilizing the empirical size–line width relation (eq. [1]) yields a derived mass-luminosity relation

$$M_{VT} = 132 \left(\frac{L_{CO}}{T_0} \right)^{4/5} (M_\odot) . \quad (12)$$

For the clouds in our catalog T_0, averaged over the entire cloud, is typically 4 K which gives

$$M_{VT} = 43 (L_{CO})^{4/5} \ (M_\odot) , \quad (13)$$

in good agreement with the empirical relation (eq. [8]). We have shown that the 4/5 exponent in the observed mass-luminosity law is a direct consequence of observing clouds in virial equilibrium obeying the size–line width relation (eq. [1]).

From equation 12 we see that the effective conversion factor from luminosity to mass is lower for hotter clouds than for cooler ones and is lower for more luminous or massive clouds. For a fixed luminosity the mass-to-luminosity ratio can be expressed as a function of the average density which scales as $\bar{\rho} \propto S^{-1}$, thus yielding

$$\frac{M_{VT}}{L_{CO}} \propto \frac{\bar{\rho}^{1/2}}{T_0} . \quad (14)$$

Thus the small scatter in Figure 2 may be interpreted as evidence of a small scatter in the mean density of the clouds at a fixed luminosity.

While the empirical virial mass–CO luminosity relation establishes a firm calibration for the molecular cloud mass in the disk of the Milky Way, our analysis shows that caution must be exercised in extending this approach to external galaxies and particularly to clouds near the centers of galaxies which may have very different densities and temperatures. Molecular clouds near the centers of galaxies require substantially higher densities than disk clouds in order to maintain stability against tidal forces. Regions of extremely active star formation will have higher temperatures. The combination of these two effects could either increase or decrease molecular mass estimates derived from CO luminosities. While the range of temperatures is likely to be small (factors of 2) due to efficient gas cooling, the range of densities may be large (10^2). Central regions in external galaxies[1] with the most dense and massive clouds will have a larger molecular hydrogen mass than that indicated by the use of the Galactic conversion factor.

The mist model of the giant molecular clouds can be carried a step further if we assume that each droplet is supported by its thermal pressure only, unlike the cloud as a whole, which is supported by the much larger velocity dispersion of the droplets. In that case the average number of droplets along a line of sight through a cloud, N_d, should be of the order of the ratio between the three-dimensional velocity dispersion of the droplets, $\sigma_v \approx 5$ km s^{-1}, and the speed of sound in each droplet, $c_s \approx 0.5$ km s^{-1}. We then have

$$N_d \approx \frac{\sigma_v}{c_s} \approx 10 .$$

If N_d is much smaller, the line profiles would breakup into several distinct lines; while if it is much larger the droplets would overlap in velocity space, the cloud would then become optically thick, and the line shape would saturate. Most of the average line profiles observed for the clouds in the catalog have Gaussian shapes. Since the beam size is greater than the droplet size for virtually all of the clouds in this survey, the number of droplets in the beam will be substantially greater than the number along the line of sight. For very nearby giant clouds, fully mapped at high-resolution, we would expect to see changes in the line profile due to the droplet statistics.

Assuming that most of the mass of a cloud is in the droplets, N_d is then simply the product of the cross section per unit mass of the droplets and the mean mass surface density of the cloud. If for simplicity we assume that the droplets are identical homogeneous spheres with density ρ_d and radius R_d we have

$$N_d = \frac{3\bar{\Sigma}}{4\rho_d R_d} ; \quad (15)$$

$$R_d = \frac{3}{4} \frac{\bar{\Sigma} c_s}{\rho_d \sigma_v} \quad (16)$$

If we adopt a characteristic value of $n(H_2) = 10^3$ cm^{-3}, which is intermediate between the mean density of the clouds $\sim 10^2$ cm^{-3} and the upper limit on the local density of $\sim 10^4$ cm^{-3} based on weakness or absence of CS emission over the cloud surface (we find CS emission only over a very small core section of the clouds), then using the empirically derived value for $\bar{\Sigma}$ and the characteristic mass of a droplet $M_d = (4\pi/3)\rho_d R_d^3$ yields

$$R_d = 0.2 \left[\frac{10^3}{n(H_2)} \right] \left(\frac{10}{N_d} \right) \text{(pc)} ;$$

$$M_d = 2 \left[\frac{10^3}{n(H_2)} \right]^2 \left(\frac{10}{N_d} \right) (M_\odot) .$$

In this mist model a giant molecular cloud then consists of $\sim 10^5$ stellar mass–sized droplets. The filling factor of the droplets is given by the ratio of the mean density of the cloud and the mean density of the droplets ~ 0.1. All of the parameters in this model are obviously tentative, and they are not required by the empirical size–line width or mass-luminosity relations which are the main results of this work. Although the model

[1] A discussion of the use of CO luminosity to determine molecular mass in external galaxies has also been given by Dickman *et al.* (1986).

appears to satisfy the constraints of optically thick emission in an optically "thin" cloud, many problems remain. In particular the droplet model leaves unanswered the question of the support of the cloud or the source of the energy input, probably feedback from star formation necessary to sustain the motion of the droplets which will collide in less than a crossing time. An elaborate treatment of the radiative transfer in a clumpy cloud model is given by Kwan and Sanders (1986).

The droplet radius (or mass) derived above is tantalizingly close to the Jeans wavelength (mass) for the density and sound speed inside the droplets

$$\lambda_J = \left(\frac{c_s^2}{4\pi G\bar{\rho}}\right)^{1/2}.$$

Most recent scenarios for gravitational instability and star formation in giant molecular clouds have used the observed velocity widths to determine the Jeans mass. The resulting masses are much larger than stellar masses, and a further process of fragmentation therefore had to be invoked. In our model star formation occurs in the droplets, and no further fragmentation is needed. Thus the thermal velocity dispersion is returned to the star-formation problem.

V. CONCLUSIONS

From an analysis of several hundred Galactic molecular clouds we have shown the following.

1. The velocity line width of giant molecular clouds is proportional to the 0.5 power of the size, $\sigma_v \propto S^{0.5}$. Combined with viral equilibrium this shows the clouds are characterized by a constant mean surface density of 170 $M_\odot$ pc^{-2} and have a mass $M \propto \sigma_v^4$.

2. The virial mass–CO luminosity law for giant molecular clouds is $M \propto (L_{CO})^{0.81}$. This establishes a calibration for measuring the total molecular cloud mass from CO observations in the disk of the Galaxy. The molecular hydrogen column density is, on average for clouds in the Galactic disk inside the solar circle, $N(H_2) = 3.0 \times 10^{20} I_{CO}$ cm^{-2}, where I_{CO} is the CO integrated intensity. The total mass of molecular clouds between $R = 2$ kpc and the solar circle is $2.0 \times 10^9\ M_\odot$.

3. The mass-CO luminosity calibration is proportional to the square root of the mean density of the clouds and inversely proportional to their temperature. Caution should be used in attempting to use this calibration for drastically different environments such as the central regions of galaxies where the density within individual clouds may be much greater than that in Galactic disk clouds, and the temperature may be higher if star formation is enhanced.

4. Molecular clouds are in or near virial equilibrium since their mass per unit CO luminosity, determined dynamically, agrees with other independent measurements. This shows that clouds are not confined by pressure equilibrium with a warm or hot phase of the interstellar medium.

5. The cloud CO luminosity is $L_{CO} \propto \sigma_v^5$. This is the molecular cloud analog of the Tully-Fisher or Faber-Jackson law for galaxies.

6. The mass-luminosity law can be accounted for by a cloud model which consists of a large number of optically thick clumps in virial equilibrium, each with a thermal internal velocity dispersion. The cloud is effectively optically thin at a fixed velocity along the line of sight. Typical droplets are of order a stellar mass and approximately equal to the Jeans mass at the density and thermal velocity dispersion of the droplets.

REFERENCES

Bhat, C. L., Issa, M. R., Houston, B. P., Mayer, C. J., and Wolfendale, A. W. 1985, *Nature*, **314**, 511.
Blitz, L., and Shu, F. H. 1980, *Ap. J.*, **238**, 148.
Bloeman, J. B. G. M., Caraveo, P. A., Hersen, W., Lebrun, F., Maddalena, R. J., Strong, A. W., and Thaddeus, P. 1984, *Astr. Ap.*, **139**, 37.
Bloeman, J. B. G. M., *et al.* 1986, *Astr. Ap.*, **154**, 25.
Bronfman, L., and Thaddeus, P. 1987, preprint.
Clemens, D. P., Sanders, D. B., Scoville, N. Z., and Solomon, P. M. 1986, *Ap. J. Suppl.*, **60**, 297.
Cohen, R. J., and Davies, R. D. 1976, *M.N.R.A.S.*, **175**, 1.
Cohen, R. S., Grabelsky, J., May, L., Bronfman, L., Alvarez, H., and Thaddeus, P. 1985, *Ap. J. (Letters)*, **290**, L15.
Dame, T. M., Elmegreen, B. G., Cohen, R. S., and Thaddeus, P. 1986, *Ap. J.*, **305**, 892.
Dame, T. 1984, Ph.D. thesis, Columbia University.
Dickman, R. L. 1975, *Ap. J.*, **202**, 50.
Dickman, R. L., Snell, R. L., and Schloerb, F. P. 1986, *Ap. J.*, **309**, 326.
Downes, D., Wilson, T. L., Bieging, J., and Wink, J. 1980, *Astr. Ap. Suppl.*, **40**, 379.
Gordon, M. A., and Burton, W. B. 1976, *Ap. J.*, **208**, 346.
Kwan, J., and Sanders, D. B. 1986, *Ap. J.*, **309**, 783.
Larson, R. B. 1981, *M.N.R.A.S.*, **194**, 809.
Liszt, H. S. 1982, *Ap. J.*, **262**, 198.
Liszt, H. S., Xiang, D., and Burton, W. B. 1981, *Ap. J.*, **249**, 532.
Myers, P. C. 1983, *Ap. J.*, **270**, 105.
Myers, P. C., Dame, T., Elmegreen, B., and Thaddeus, P. 1986, preprint.
Rivolo, A. R., Solomon, P. M., and Sanders, D. B. 1986, *Ap. J. (Letters)*, **301**, L19.
Sanders, D. B., Clemens, D. P., Scoville, N. Z., and Solomon, P. M. 1986, *Ap. J. Suppl.*, **60**, 1.
Sanders, D. B., Scoville, N. Z., and Solomon, P. M. 1985, *Ap. J.*, **289**, 373.
Sanders, D. B., Solomon, P. M., and Scoville, N. Z. 1984, *Ap. J.*, **276**, 182.
Scoville, N. Z., and Solomon, P. M. 1975, *Ap. J. (Letters)*, **199**, L105.
Solomon, P. M., and Sanders, D. B. 1980, in *Giant Molecular Clouds in the Galaxy*, ed. P. M. Solomon and M. G. Edmunds (New York: Pergamon), p. 41.
Solomon, P. M., Sanders, D. B., and Rivolo, A. R. 1985, *Ap. J. (Letters)*, **292**, L19.
Solomon, P. M., Sanders, D. B., and Scoville, N. Z. 1979, in *IAU Symposium 84, The Large Scale Characteristics of the Galaxy*, ed. W. B. Burton (Dordrecht: Reidel), p. 35.
Solomon, P. M., Sanders, D. B., Scoville, N. Z., and Clemens, D. P. 1987, *Ap. J. Suppl.*, in press.
Solomon, P. M., Scoville, N. Z., and Sanders, D. B. 1977, *Ap. J. (Letters)*, **232**, L89.
Stark, A. A. 1979, Ph.D. thesis, Princeton University.
Thaddeus, P., and Dame, T. M. 1984, *Workshop on Star Formattion*, in *Reports of Royal Observatory, Edinburgh*, ed. R. Wolstencroft.

J. M. BARRETT, P. M. SOLOMON, and A. YAHIL: Astronomy Program, Department of Earth and Space Sciences, State University of New York, Stony Brook, NY 11794

A. R. RIVOLO: Department of Astronomy and Astrophysics, University of Pennsylvania, Philadelphia, PA 19104-6394